Gas Transfer and Liquid Dispersion Inside a Deep Airlift Reactor

J. P. Giovannettone
Institute of Water Resources-Hydrologic Engineering Center, U.S. Army Corps of Engineers, Davis, CA 95616

J. S. Gulliver
Saint Anthony Falls Laboratory, Dept. of Civil Engineering, University of Minnesota, Minneapolis, MN 55455

DOI 10.1002/aic.11449
Published online February 21, 2008 in Wiley InterScience (www.interscience.wiley.com).

Gas transfer experiments in bubbly flow are conducted inside a deep bubble column/airlift reactor containing air and water with a maximum aerated water height of 23.4 m and diameter of 1.06 m. The effects of geometry and operating conditions on mixing and gas transfer are determined. Fluorescence measurements are used to estimate dispersion coefficients for several operating conditions, while bubble-water gas transfer measurements are made using dissolved oxygen (DO) probes. A two-phase convection-dispersion model is fit to the DO measurements using the liquid film coefficient (k_L) as a fitting parameter. Sparger differences had a substantial effect upon k_L, and the gas transfer coefficient for the airlift reactor was four times that of the bubble column. Results are characterized using Sherwood, Reynolds, and Bond numbers. A low Reynolds number exponent was found, indicating that k_L in a deep column tends toward a constant and is not highly dependent upon air discharge. © 2008 American Institute of Chemical Engineers *AIChE J,* 54: 850–861, 2008
Keywords: bubble column, airlift reactor, gas–liquid systems, gas–liquid mass transfer, dispersion, aeration

Introduction

Bubble columns and airlift reactors up to 40 m in height and 10 m in diameter are used in industry for the catalytic conversion of hydrocarbons, coal liquefaction, or the synthesis of hydrocarbons from carbon monoxide and hydrogen, absorption processes, extraction, fermentation, among others. In these reactors, there are three types of gas–liquid flows that occur: (1) bubbly flow, where individual bubbles rise with or against the flowing liquid; (2) slug flow, where a bullet shaped Taylor bubble rises at high velocity while shedding smaller bubbles; and (3) annular flow, where a liquid film rises along the wall with a gas core. Depending upon the goals and operating conditions of the reactor, industrial columns may operate in any of the three operating regimes or in the transitions between these regimes.

There is one important application that operates exclusively in the bubbly flow regime. That would be the use of an airlift reactor to add oxygen to the bottom of a lake or reservoir that replenishes the low levels of dissolved oxygen (DO) that occur in the hypolimnion.[1] An airlift reactor used in lakes and reservoirs (hypolimnetic reactor) consists of a riser that takes in unaerated water through the middle of the device and an outer shell, where the newly aerated water is returned to the bottom of the water body. The environmental benefits of aeration and oxygenation systems include preventing algal blooms, promoting the survival of aerobic bacteria, decreased carbon dioxide concentrations, odor prevention through the oxidation of hydrogen sulfide, and improved living conditions for fish and other aquatic life.

The popularity of bubble columns, especially in chemical engineering applications, is associated with their easy

Correspondence concerning this article should be addressed to J. S. Gulliver at gulli003@umn.edu.

construction, lack of moving parts, and inexpensive maintenance. Airlift reactors have recently been adopted because they also allow higher circulation rates, where the liquid flow can be more easily controlled than in the traditional bubble column. Airlift reactors differ in that the rising fluid (contained in the riser) is separated from the sinking fluid (contained in the downcomer). A headspace exists near the top, where the riser and downcomer join to allow the gas to escape.

Because of the various applications of airlift reactors and bubble columns, studies have been performed in an attempt to link the geometry and operating conditions of the column to the efficiency of gas transfer. The main hydrodynamic characterization parameters are the gas void ratio, mean bubble diameter, mixing, the volumetric gas transfer rate, and the liquid circulation velocity (airlift reactors). The geometry of a reactor is described by the height and width of the column, while the operating conditions that most affect the hydrodynamics are the gas and liquid flow rates. The type of media present inside the reactor and the sparger used to introduce gas into the media are also important considerations.

The focus of the current study will concern the effects of changing the geometry and operating conditions of a full scale airlift reactor operating in the bubbly flow regime on the liquid film coefficient. The greater height of the column used will provide less concern for scaling errors. The governing one-dimensional (1D) relation in the column is given as:

$$(1-\phi)\frac{\partial C}{\partial t} + u_l \frac{\partial C}{\partial z} = (1-\phi)D_L \frac{\partial^2 C}{\partial z^2} + k_L a(C^* - C), \quad (1)$$

where C is constituent concentration in the liquid, ϕ is void fraction (volume of bubbles/total volume), u_l is the superficial liquid velocity (liquid discharge per cross-sectional area), a is the specific interfacial area of the bubbles, C^* is the liquid concentration in equilibrium with the bubbles, t is time, and z is vertical distance from the bottom of the column. The results from previous experiments in the same column[2] show that void fraction is small relative to the total volume of the reactor. Void fraction was therefore neglected in solutions of Eq. 1. Estimates of the longitudinal dispersion coefficient, D_L are made from curve fits of Eq. 1 to nonvolatile tracer concentration measurements with $k_L = 0$. Estimates of the liquid film coefficient are then made from a curve-fit of the DO measurements. All operating conditions, excluding media type and column diameter, will be tested. Prior measurements of void fraction and bubble diameter allow calculations of interfacial surface area of the bubbles to be incorporated into estimates of the liquid film coefficient and dispersion coefficient from concentration measurements over time and distance. The results will give an indication of the accuracy of previous experiments in smaller columns concerning trends in the liquid film coefficient with geometry, sparger type, and gas flow rate.

Previous Work

Several studies have been performed to estimate the gas transfer coefficient, $k_L a$, in small airlift reactors and bubble columns. The most common method is a disturbed equilibrium technique, where equilibrium of one dissolved gas compound is disturbed and the rate at which dynamic equilibrium (steady state) is approached is related to the gas transfer coefficient which is fit to the resulting compound profiles as they approach steady state.

It has been found that dissolved gas concentrations increase rapidly with measurement height above the column bottom in a region just above the sparger, while beyond this region the rate of concentration increase slows.[3] Some studies have also shown that an increase in total unaerated height, or diffuser depth, will increase gas transfer rates at lower depths in the column due to an increase in hydrostatic pressure.[4–6] Unaerated height in this context refers to the total height of the water column while the aerator is off, while the aerated height will refer to the total water column height during aeration. It is uncertain whether industrial scale columns need a more complex model for $k_L a$ that includes height variations. These models do require a complete mass balance on the bubbles and the water in the column.[7] The geometry of the column also affects the ratio of gas transfer that occurs from the bubbles and the amount that is due to the turbulence at the free surface of the tank. It was found that in a 3.4 m^2 rectangular tank with a depth of 1.1 m about one-third of oxygen absorption occurs at the surface.[8]

Higher $k_L a$ values occur at higher gas flow rates.[3–5,9–16] Many of these studies have shown the relationship to be almost linear, although Alvarez-Cuenca et al.[3] found this to be true only for a limited range of gas velocities. Wongsuchoto et al.[16] also determined k_L and a individually and found that k_L does not change with superficial gas velocity (u_g), while a does change.

It has been found that $k_L a$ increases with an increase in the number of pores or a decrease in the size of the sparger pores.[4,6,12] Ohkawa et al.[17] found the opposite trend to be true in terms of pore size, while Wongsuchoto et al.[16] found pore number to have a negligible effect. In contrast, Bovonsombut et al.[10] found that $k_L a$ increases up to superficial gas velocities of 0.0042 m/s, and decreases at higher gas velocities.

As seen from the above studies, there seems to be mixed results on what effects operating conditions and column geometry have on gas transfer rates in bubble columns and airlift reactors. The tallest column of these studies is 10.6 m in height,[18] while most are 1–2 m. The scale of commercial/field columns is up to a height of 40 m, which presents scale-up concerns with these experimental studies. The maximum column height of 23.4 m in the current study is designed to address some of these issues for the bubbly flow regime. The effects of total column height, sparger type, and column type on mixing and gas transfer will be tested in a field-scale column. Bubble surface area has been determined for these experiments,[2] allowing the liquid film coefficient to be determined under various operating conditions.

Experimental

A schematic of the reactor used in the experiments is shown in Figure 1. The shorter arrows in the figure represent the flow of water during operation of the airlift reactors. Water flows up the main column from which it exits through one of three downcomers, depending on the airlift reactor

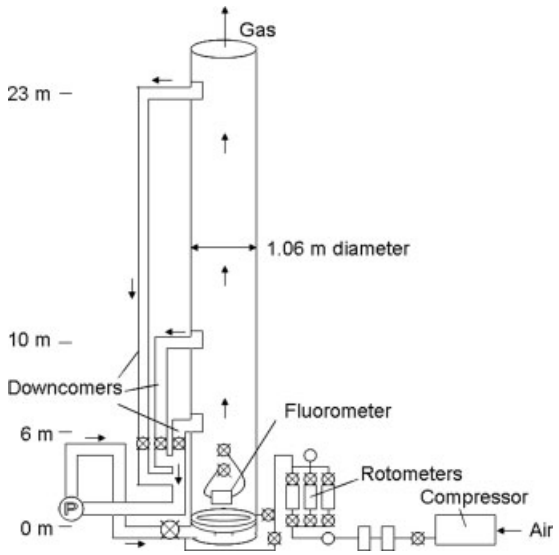

Figure 1. Schematic of reactor setup for gas transfer experiments.

size desired. It then flows down the downcomer pipe and through a pump, after which it reenters the riser below the sparger. During operation of the bubble column, the valves to the downcomers are closed so that there is no water recirculation, while the setup remains a batch system.

Three spargers are tested: a soaker hose (Figure 2a), perforated plate, and coarse bubble diffuser (Figure 2b). The soaker hose has the smallest and the greatest number of pores, while the coarse bubble diffuser has the fewest and largest pores. Flourescein dye was used as a conservative tracer inside the column to quantify the dispersion coefficient. The tracer was injected either at the top or bottom of the column, depending on the total unaerated height. When the height was set at 6.6 or 10.6 m, 5–10 mL of tracer was injected at the bottom of the column through a small tap; for experiments at 23.4 m, during which the hydrostatic pressure at the bottom of the column was much greater, the tracer was injected at the top of the downcomer. The residence time of the downcomer, however, was only on the order of 3–11 s, depending on the total height of the column. Superficial liquid velocity was held constant at 0.02 m/s. Continuous measurements of the fluorescence in the water were taken using the flow-through module of a Turner Designs10-AU fluorometer. The water was sampled at a height of 2.10 m and returned to the same liquid cross-section while taking into account the liquid flow rate, which corresponded to a height of 0.36 m above the sampling height. Bubbles were prevented from coming into the fluorometer by attaching an inverted cone to the end of the sampling tube. The resulting profiles were fit to a mass transport model to determine the dispersion coefficients for the airlift reactor and the bubble column, respectively.

The method used to estimate gas transfer rates involves initially stripping the oxygen out of the water and then reoxygenating the column, while taking continuous DO measurements at predetermined heights. Deoxygenation was accomplished by adding enough sodium sulfite with cobalt chloride as a catalyst to the column to bring the DO concentration to near 0 mg/L. The concentration of oxygen was never brought down to zero, so that it can be assumed that all of the sodium sulfite is consumed in the degassing process. In addition, the water in the column was replaced frequently to minimize any potential residual effects. Tests on the sodium sulfite–cobalt chloride dose technique have shown that sodium sulfite reacts within a few minutes when the catalyst is present unless the DO is depleted.[19] Two to five YSI Model 5739 DO probes were positioned at different depths in the column, depending on the total column height. The pump was run for 45 min at the beginning of each set of experiments to insure well-mixed conditions in terms of temperature, DO, and dissolved nitrogen (DN). DN concentration can be determined by subtraction of DO from total dissolved gases (TDG) measurements. The TDG was measured near the top of the column using an Alpha Designs Tensionometer T390^{TM} before the gas was turned on and after it was shut off. The TDG meter requires up to 15 min to reach steady state, so it was not helpful during the transient period. After the first TDG measurement was taken, all DO probes were calibrated in a 5-gal bucket filled with tap water and saturated with gas using an air pump. The probes were then positioned at the desired measurement heights in the reactor. Air was injected into the column at the desired flow rate, and DO concentration profiles were taken until a steady-state DO concentration was approached.

Model

Dispersion

The goal of the dispersion experiments is to quantify the axial mixing present in the column for specific geometrical and operating conditions. Liquid mixing in the column has been shown to be caused by three processes: convective

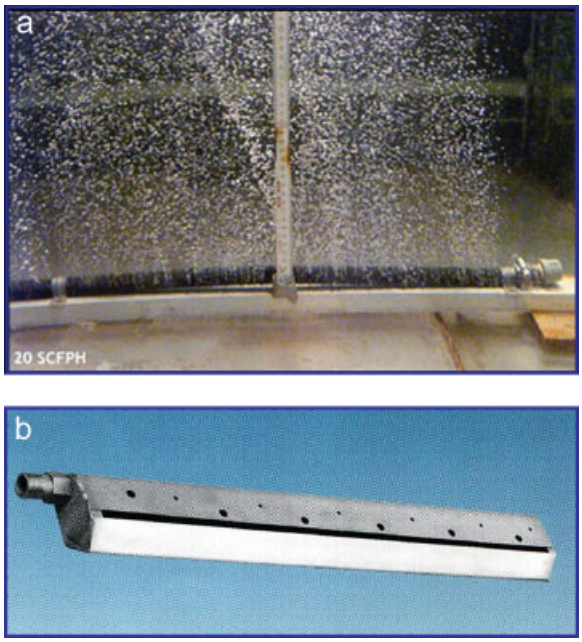

Figure 2. Pictures of a (a) soaker hose sparger and a (b) coarse bubble diffuser.

[Color figure can be viewed in the online issue, which is available at www.interscience.wiley.com.]

recirculation of the liquid phase up the center of the column and down the sides, turbulent diffusion that occurs in the wake of the rising bubbles, and molecular diffusion.[20] The 1D axial dispersion model places these factors into one dispersion coefficient (D_L). Equation 1 was used with C being the tracer concentration and $k_L = 0$.

For a bubble column, $u_l = 0$. Then the solution of Eq. 1, with the boundary conditions $\partial C/\partial t. = 0$ at $z = 0$ and $z = h_r$, where h_r is the unaerated water height of the column, and the initial conditions $C(z,0) = C_{in}$ for $0 \le z \le \gamma$ and $C(z,0) = 0$ for $z \ge \gamma$, where γ is the thickness of the initial layer of dye injected into the column, is:[21]

$$C = C_{ss}\left(1 + 2\sum_{i=1}^{\infty}\left[\cos\left(i\pi\frac{z}{h_r}\right)\exp\left(-\frac{i^2\pi^2}{h_r^2}D_L t\right)\right]\right). \quad (2)$$

In this equation, C_{ss} is the steady-state tracer concentration. Each tracer concentration profile for the bubble column setup was fit to Eq. 2 to determine D_L.

The solution of Eq. 1 for an airlift reactor with nonzero u_l, while taking into account the recirculating flow and open end boundary conditions,[22] is:

$$C = C_{ss}\sum_{i=1}^{I}\left[\left(\frac{\mathrm{Bo}t_r}{4\pi t}\right)^{1/2}\exp\left(-\frac{(z + ih_r - u_l t)^2}{4u_l h_r t}\mathrm{Bo}\right)\right], \quad (3)$$

where $\mathrm{Bo} = u_l h_r/D_L$ is the Bodenstein number and t_r is the recirculation time. Each tracer concentration profile from the airlift reactor experiments was fit to Eq. 4 to determine D_L.

Gas transfer

The assumptions that are required in most analytical and numerical models of gas transfer are (1) that k_L and a are estimated as one parameter and (2) that gas concentrations of both oxygen and nitrogen in the bubble are constant over time and space. The latter assumption simplifies the model, but may not be appropriate for a deep bubble column. The current model will not require these assumptions, and will complete the mass balance by considering changes in oxygen and nitrogen concentration in the bubbles and in the water column. To model DO concentrations in the water while taking into account the gas concentrations of oxygen and nitrogen in the bubbles, the change in the concentration of DN in the water needs to be determined or assumed.[7,17] The equations for oxygen and nitrogen used to develop the gas-transfer model use Eq. 1 for each constituent:

$$(1-\phi)\frac{\partial C_O}{\partial t} + u_l\frac{\partial C_O}{\partial z} = D_L\frac{\partial^2 C_O}{\partial z^2} + k_L a(C_O^* - C_O) \quad (4)$$

$$(1-\phi)\frac{\partial C_N}{\partial t} + u_l\frac{\partial C_N}{\partial z} = D_L\frac{\partial^2 C_N}{\partial z^2} + \left(\frac{D_N}{D_O}\right)^{0.5} k_L a(C_N^* - C_N), \quad (5)$$

where C is the concentration in the water, C^* is the concentration of the water in equilibrium with the gas in the bubble, a is the bubble surface area per unit volume of liquid–gas mixture, k_L is the liquid film coefficient for oxygen, D is a diffusion coefficient, and subscripts O and N indicate oxygen and nitrogen, respectively. The liquid film coefficient for nitrogen is assumed to be equal to k_L times the respective ratio of diffusion coefficient to the $^1/_2$ power.[23] A third constituent equation could be added to Eqs. 4 and 5 if desired. In addition, Eqs. 4 and 5 could be replaced if the respective constituent does not exist in either the gas or the liquid.

The model used in this study to solve Eqs. 4 and 5 is based on an explicit computational mass transport scheme. The column is split into 10, 15, or 35 control volumes, depending on the total height tested, in which the DO and DN fluxes and concentrations are estimated for each time step. The convection and dispersion terms were calculated for each control volume using upstream and central differences, respectively. This is due to the fact that convection is controlled by the upstream control volume, whereas dispersion is controlled by both the upstream and downstream control volumes. The following boundary conditions were used:

1. At $z = 0$, $D_L\frac{\partial C}{\partial z} = 0$, $y = 0.266$, and $C_{z=0} = C_{z=L}$
2. At $z = h_r$, $D_L\frac{\partial C}{\partial z} = 0$, and the free-surface transfer terms, $k_L a_S(C_{SO} - C_O)$ and $k_{LN} a_S(C_{SN} - C_N)$, were added to Eqs. 4 and 5, respectively.

The variable y represents the molar ratio of oxygen to nitrogen concentrations in the bubble. The value of the surface transfer coefficient, $k_L a_S$, is computed using a relation developed by Schierholz et al.[6] for sparged liquids:

$$\frac{k_L a_S}{k_L a} = 1.85\left(k_L a\frac{V}{Q_g}\right)^{0.92}, \quad (6)$$

where V is the column volume and Q_g is the gas flow rate.

At the beginning of each model run, the dispersion number (Di) and the Courant number (Co) were calculated to insure stability in the results:

$$\mathrm{Di} = \frac{D_L\Delta t}{\Delta z^2} \quad (7)$$

$$\mathrm{Co} = \frac{U\Delta t}{\Delta z}, \quad (8)$$

where Δt and Δz are the time interval and chamber length, respectively, and U is the characteristic gas or liquid velocity in the system. Courant numbers for both the liquid and the gas were calculated using the superficial liquid velocity and the bubble rise velocity. The dispersion number must remain below 0.5 and the Courant number below 1 to maintain stability in the model. Using the values of D_L determined in the dispersion experiments and values of 2.0 s and 0.7 m for Δt and Δz, respectively, Di ranged from 0.12 to 0.37. Using the same values for Δt and Δz, the Courant number for the liquid was 0.06 and for the gas 0.77. All values were within the stability range.

To close the mass balance for oxygen and nitrogen, the vertical profile of y is computed. This was done using an equation developed by McWhirter and Hutter[5] and adapted by DeMoyer et al.[7] to incorporate the transfer of nitrogen gas into and out of the bubbles. The expressions for the concentration of oxygen and nitrogen in the bubble, are, respectively:

$$V_b\frac{dC_{Ob}}{dt} = -k_{LO}A_b(C_O^* - C_O) \quad (9)$$

$$V_b\frac{dC_{Nb}}{dt} = -k_{LN}A_b(C_N^* - C_N). \quad (10)$$

The expansion of dy/dz is:

$$\frac{dy}{dz} = \left(\frac{1}{C_{Nb}}\frac{\partial C_{Ob}}{\partial z} - \frac{C_{Ob}}{C_{Nb}^2}\frac{\partial C_{Nb}}{\partial z}\right). \quad (11)$$

For most conditions, the gas concentration change over time is small relative to the change over depth, therefore $\partial C/\partial t \rightarrow 0$ and:

$$\frac{dC}{dt} = \frac{\partial C}{\partial z} \cdot U_r. \quad (12)$$

Equation 11 can then be rewritten using Eqs. 9, 10, and 12 as:

$$\frac{dy}{dz} = -\left(\frac{k_{LO}A_b}{V_b U_r}\frac{1}{C_{Nb}}\left(C_O^* - C_O\right) - \frac{k_{LN}A_b}{V_b U_r}\frac{C_{Ob}}{C_{Nb}^2}\left(C_N^* - C_N\right)\right). \quad (13)$$

The gas concentration in the bubble can be related to the liquid gas concentration using Henry's Law:

$$C_b = H \cdot C^*, \quad (14)$$

and $V_b U_r$ can be expressed as measureable quantities using the definition of residence time (t_r):

$$t_r = \frac{h}{U_r} = \frac{V_b}{Q_g}. \quad (15)$$

Substituting Eqs. 14 and 15 into Eq. 13 and using the assumption that the liquid film coefficient for nitrogen is equal that of oxygen times the respective ratio of diffusion coefficient to the $^1/_2$ power,[23] a final expression for dy/dz can be formed:

$$\frac{dy}{dz} = -k_L a \frac{A_r}{Q_g} \times \left(\frac{1}{H_N C_N^*}\left(C_O^* - C_O\right) - \left(\frac{D_N}{D_O}\right)^{1/2}\frac{H_O C_O^*}{\left(H_N C_N^*\right)^2}\left(C_N^* - C_N\right)\right), \quad (16)$$

where A_r is the cross-sectional area of the reactor. Equation 16 disaggregates temporal from spatial variations in molar ratio because temporal, relative to spatial, variations are small. The variables C_O^* and C_N^* for each chamber are calculated using the following equations:[7]

$$C_O^* = C_{SO}\frac{P_{atm} - P_{vapor} + (\rho_l g(h_r - z))}{P_{atms} - P_{vapor}}\left(\frac{y/(1+y)}{0.21}\right) \quad (17)$$

$$C_N^* = C_{SN}\frac{P_{atm} - P_{vapor} + (\rho_l g(h_r - z))}{P_{atms} - P_{vapor}}\left(\frac{1/(1+y)}{0.79}\right), \quad (18)$$

where C_{SO} and C_{SN} are the saturation concentrations of oxygen and nitrogen in the liquid at water temperature and atmospheric pressure, respectively, P_{atm} is local atmospheric pressure, P_{atms} is atmospheric pressure at standard conditions, P_{vapor} is the vapor pressure, and ρ_l is the liquid density. At $z = 0$, $y = 0.266$ is known, and Eqs. 17 and 18 can be computed along with Eqs. 4 and 5, by ignoring convection and dispersion in the first time step (5 s). In Eqs. 4 and 5, an initial nitrogen concentration was determined by subtracting the initial DO concentration in the water from the TDG measurement taken before the start of each experiment. A value for k_L is also chosen. The DO and DN concentrations can then be computed in the first chamber during the first time step using the initial DO and DN concentrations in the water and $\partial C_O/\partial t$ and $\partial C_N/\partial t$ from Eqs. 4 and 5. The newly calculated DO and DN concentrations are used to determine a new dy/dz. A fourth-order Runge–Kutta Method was then used to determine y in the second chamber from dy/dz just calculated in the first chamber. It was found that two iterations of these computations were required before y converged on a single value. The value of y is then used to calculate C_O^* and C_N^* in the second chamber, which are then used to calculate $\partial C_O/\partial t$ and $\partial C_N/\partial t$ and estimates of DO and DN concentrations in the next time step. The gradient dy/dz is computed for the second chamber, and the process is repeated for the third chamber up to the top chamber. For the next time step, DO and DN concentrations in each chamber are computed using the values of $\partial C_O/\partial t$ and $\partial C_N/\partial t$ from the previous time step for each corresponding chamber. The process described above is repeated for all chambers and for all time steps.

The model is set up so that gas transfer does not occur ($k_L = 0$) in a chamber until the bubbles reach that chamber. The bubbles are assumed to have a maximum rise velocity of 0.27 m/s, which is the velocity of the liquid (~0.02 m/s) added to the approximate slip velocity of the bubbles (~0.25 m/s). As the bubbles rise, k_L is set to a nonzero value for the corresponding chambers. A single value of k_L is chosen for the column so as to minimize the root mean square value of the difference between the data and model calculations at each DO measurement height.

Results and Discussion

Dispersion

Figure 3 provides typical tracer measurements obtained without gas flow, along with the curve fits to Eq. 3. It can be seen that the first peak is not fit well, but after this initial peak the fit improves. When fitting the tracer concentration data to Eqs. 2 or 3, it was difficult to predict the initial peak, which is likely due to the time it takes for the peak to develop and the tracer to become cross-sectionally well-mixed.

Figure 4 provides the variation with superficial gas velocity of the dispersion and diffusion coefficients for the airlift reactor and bubble column, respectively, under various column heights. Also shown are curve-fits of these results used to represent longitudinal dispersion in the computational model. As other studies have shown,[5,11,21,24] the dispersion coefficient increases with superficial gas velocity to a power less than 1. Figure 4 also indicates that mixing increases as the total unaerated height of the airlift reactor increases. This is contrary to the findings of Fields and Slater[25] and Gavrilescu and Tudose[26] for smaller reactors. The amount of mixing induced throughout the reactor by the coarse bubble diffuser and the perforated plate were similar, while the soaker hose caused less mixing at superficial gas velocities greater than 0.004 m/s. It was found that the soaker hose had a more uniform bubble size than the other spargers,[2] and it is believed that the presence of a few large bubbles produced

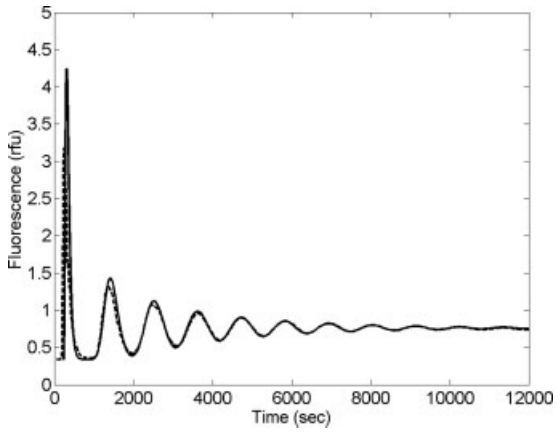

Figure 3. Example dye concentration profile (dotted line) and best fit according to Eq. 4 (solid line) for no gas flow in the airlift reactor using a perforated plate and a total unaerated height of 23.4 m.

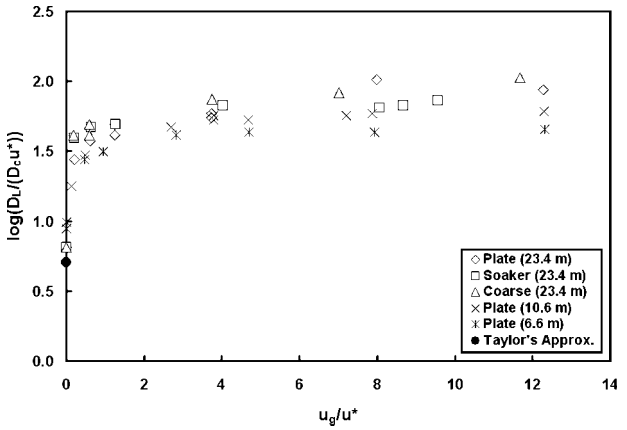

Figure 5. Comparison of dispersion results with Taylor's equation for dispersion in a fully developed turbulent flow with a logarithmic velocity profile.

by the perforated plate and coarse bubble diffusers with larger rise velocities causes an increase in axial dispersion coefficient.

A comparison is also made between the 23.4-m airlift reactor and bubble column. The bubble column experiences greater mixing at all superficial gas velocities tested, which is in agreement with the results of Gavrilescu and Tudose.[26] A minimum amount of dispersion in the bubble column was observed at gas velocities near 0.003 m/s, while a maximum was seen at 0.001 m/s. At low superficial velocities there may have been a "bubble cap" flow regime set up in the bubble column, which would have increased longitudinal mixing, while at higher superficial gas velocities, the bubbles may be more evenly distributed laterally, reducing the longitudinal mixing.

Figure 5 provides the airlift reactor results in dimensionless form compared to the result from Taylor's[27] relation for D_L in a single-phase, turbulent pipe flow, $D_L/(u^* D_c) = 5.05$, where D_c is the column diameter and u^* is the shear velocity near the walls. The value of u^* is estimated using the Darcy–Weisbach friction factor, $f = 0.027$, corresponding to a u_l of 0.02 m/s and a wall roughness between hydraulically smooth and 1 mm. This wall friction approximation should also be valid for the two-phase flow cases in the present study because of the low void ratios used. It can be seen that the single-phase results correspond with the predictions of Taylor.

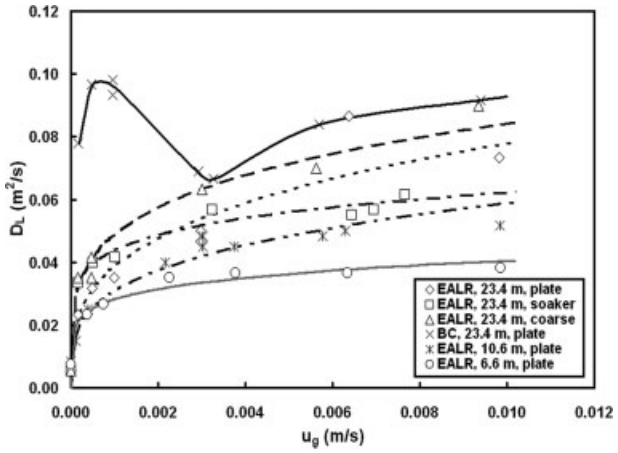

Figure 4. Dispersion coefficients for all sets of operating conditions.

The bubble column cross-sectional mean velocity is zero, thus turbulent diffusion coefficients are given.

Liquid film coefficient (k_L)

The total column height and operating conditions tested for each experiment are given in Table 1. An example set of profiles is shown in Figure 6 for the bubble column and perforated plate operating at an unaerated height of 23.4 m and a superficial gas velocity of 0.01 m/s. The time lag after the initial bubbles were released but before gas transfer occurred at each height varied with dispersion coefficient and superficial gas velocity and was well-simulated in the computational model. It can also be seen that the steady-state oxygen concentration decreases from deeper to shallower depths.

The DO concentrations measured near steady-state are provided in Figure 7 at each measurement height and superficial gas velocity. Measurements of DO were taken between 15 and 20 min after the gas was turned on. The various line types represent the different superficial gas velocities tested, while the solid line serves as a guide of the equilibrium concentration of oxygen with air bubbles at depth. At low depths in the column, the DO concentration is below equilibrium, suggesting a positive gas transfer rate from the bubbles into the water. This oxygen deficiency is more extreme at lower superficial gas velocities, where there is less mixing. Near the upper portion of the column, DO concentrations are above equilibrium, especially for the higher gas flow rates. This effect is more clearly seen when using the 23.4-m airlift reactor (Figures 7a–c). The recirculating liquid brings the higher concentrations from near the bottom of the column up

Table 1. Designation (Column 1) and Description of DO Experiments Performed in the Current Study Including Total Column Height, Superficial Liquid Velocity, Sparger Type Used, Superficial Gas Velocity, Water Temperature, and Kinematic Viscosity

Exp.	Column Height (m)	u_l (m/s)	Sparger Type	$u_g \times 10^3$ (m/s) at STP	T(°C)	$v \times 10^6$ (m^2/s)
P1	23.4	0.02	Plate	1.0	20.6	0.989
P2	”	”	”	3.1	16.9	1.087
P3	”	”	”	5.3	19.7	1.010
P4	”	”	”	10.4	15.2	1.213
S1	”	”	Soaker	0.6	19.5	1.016
S2	”	”	”	1.2	18.5	1.043
S3	”	”	”	3.8	15.7	1.120
S4	”	”	”	8.0	15.8	1.117
C1	”	”	Coarse	1.0	21.5	0.968
C2	”	”	”	3.0	20.0	1.002
C3	”	”	”	4.9	14.8	1.146
C4	”	”	”	9.9	16.6	0.986
P5	”	0	Plate	1.0	18.0	1.057
P6	”	”	”	3.1	13.0	1.206
P7	”	”	”	5.0	13.5	1.189
P8	”	”	”	9.9	18.2	1.051
P9	10.6	0.02	”	0.8	22.0	0.957
P10	”	”	”	2.5	22.3	0.950
P11	”	”	”	4.2	22.3	0.950
P12	”	”	”	6.0	22.4	0.948
P13	”	”	”	11.0	22.6	0.944
P14	6.6	”	”	0.7	30.1	0.798
P15	”	”	”	2.3	29.3	0.811
P16	”	”	”	3.8	29.3	0.811
P17	”	”	”	5.3	31.4	0.778
P18	”	”	”	9.7	29.3	0.811

closer to the top. The effect is not as clear in the shorter airlift reactors (Figures 7d, e) due to a smaller difference between bottom and top concentrations, and in bubble columns (Figure 7f) where there is no recirculation velocity. This suggests a negative gas transfer rate from the water into the bubbles. Near the top of the column in some instances (Figures 7a, b, e, and f) the DO concentration is higher for the lowest superficial gas velocity than during experiments when the gas flow rate was increased. This may be due to a loss of gas from the liquid to the air at the water surface where increased gas flow rates will cause greater amounts of turbulence and mixing with the air. The net area between each curve and the solid line should be close to zero at steady-state, because there would be no overall net transfer of oxygen between the water and the bubbles, with the following caveats: (1) If the k_La values are larger at the top than at the bottom of the column, the area between the curves would be smaller at the top of the column, (2) The bubble-water oxygen transfer coefficient is 6% larger than that for nitrogen gas, which would cause a slight horizontal sag in the equilibrium line, and (3) the temperature is variable between experiments, although not substantially, which would cause the equilibrium line to shift horizontally. The mean temperature of the experiments in each figure was used to compute the solid line. The measured profiles of DO in Figure 7 indicate that these caveats had a significant effect, because the net area is weighted toward the bottom of the column. The likely reason is that specific surface area is larger at the top than at the bottom of the column. In addition, the low gas transfer relative to longitudinal mixing in the column is apparent at low superficial gas velocities in Figure 7 where the DO profiles approach vertical.

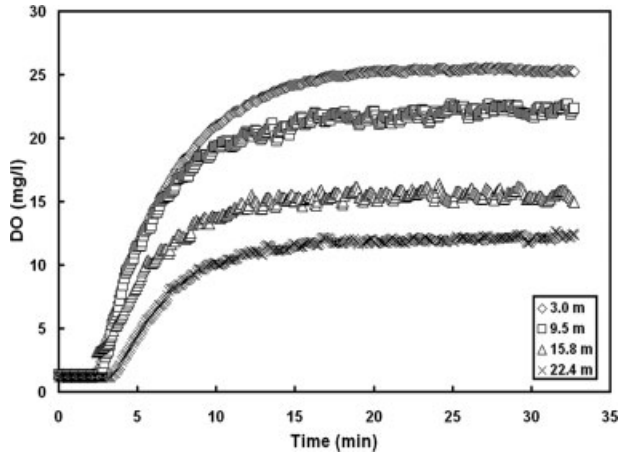

Figure 6. DO concentration profiles taken at various measurement heights in the 23.4-m airlift reactor using the perforate plate as a sparger at u_g = 0.01 m/s.

Profiles of y at different depths were also computed under the operating conditions of the experiments and plotted in Figure 8 to determine whether it is necessary to close the mass balance on oxygen and nitrogen concentrations in the bubble. It can be seen that at times under 20 min for the bubble column (or a bottom constituent concentration of less than 75% of C^*), the change in y with height is substantial. In a bubble column or airlift reactor of any height that will be operated in an unsteady mode, it is necessary to be able to predict the variation of y with height during this initial period. This result also suggests that the variation of y with height may be substantial if a reactor is operated in steady state with an inflow concentration less than 75% of its local equilibrium.

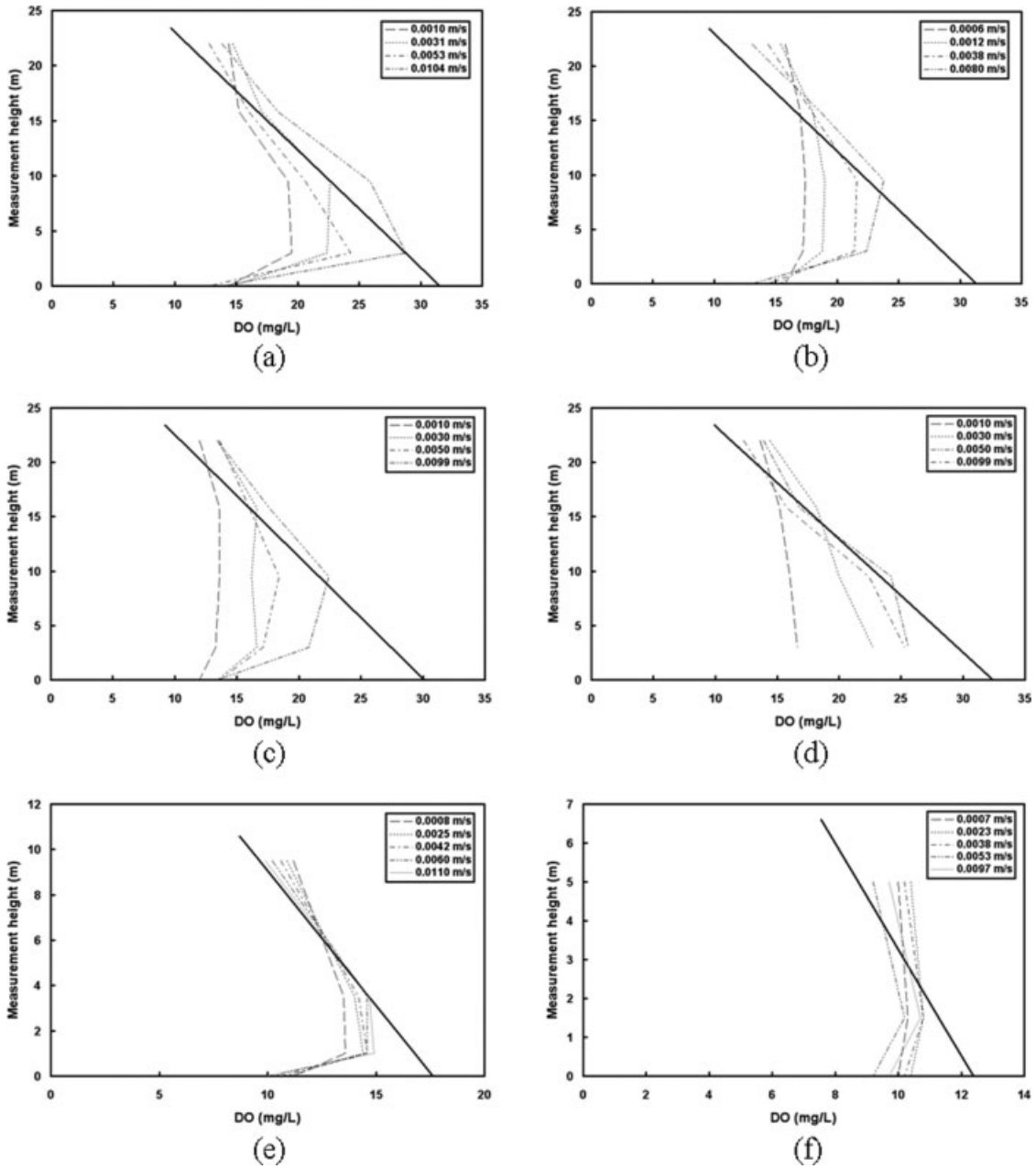

Figure 7. DO measurements for various superficial gas velocities throughout the height of the column compared to the line of saturation (solid line).

Six operating conditions are shown (column type/total unaerated height/sparger): (a) airlift reactor/23.4 m/plate, (b) airlift reactor/23.4 m/soaker hose, (c) airlift reactor/23.4 m/coarse, (d) BC/23.4 m/plate, (e) airlift reactor/10.6 m/plate, and (f) airlift reactor/6.6 m/plate.

To determine the fitted k_L, the volumetric interfacial surface area of the bubbles (a) was calculated using the equation for spherical bubbles:[28]

$$a = \frac{6\phi_g}{d_b} \tag{19}$$

where d_b is the Sauter mean bubble diameter. Estimates of void ratio and bubble diameter were made in a previous study[2] through measurements of pressure differences between specific column heights and a submersible camera and strobe light attached to a vertical trolley, respectively. Calculations assuming ellipsoidal bubbles[29] were found to increase the surface area by 4.9%. This is believed to be small compared to the experimental uncertainties that exist with these techniques, and, therefore, all calculations assumed spherical bubbles.

The computational model of Eqs. 4 and 5 was then used to fit $k_{L,}$ assuming k_L is constant with height. A typical example of the model fit (solid line) to the data is given in Figure 9. The model was fit by choosing a k_L that minimizes the error between the data and the model at specific points.

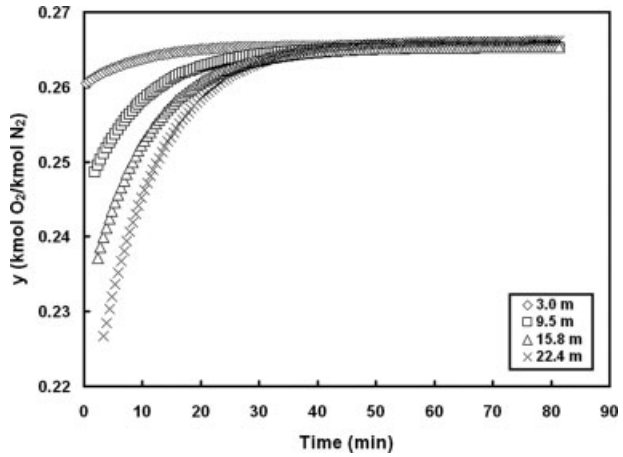

Figure 8. Computed profiles of *y* taken at various measurement heights in the 23.4-m bubble column using the perforated plate as a sparger at u_g = 0.01 m/s.

These points are represented as open circles on the data plot of Figure 9. They were chosen every 20 s after the initial increase in DO concentration in order to emphasize the results of the unsteady period, for a total of 300 s, and every 100 s afterward. The final results are given in Table 2. Values of k_L were lower than those found by Wongsuchoto et al.,[16] where k_L was estimated to be 4.1×10^{-4} m/s for all operating conditions in a 1.2-m tall airlift reactor. The values of k_L do compare well with the values found by Kataoka et al.[30] for a 9-m tall bubble column and are also within the ranges predicted by equations developed by Calderbank and Moo-Young[31] and Akita and Yoshida[32] for superficial gas velocities in the bubbly regime, but higher than those found here.

It can be seen in Table 2 that k_L is highest for the airlift reactor using the perforated plate and lowest for the airlift reactor with the coarse bubble diffuser and the bubble column with the perforated plate, which is consistent with other studies.[9,11,13,14] Considering the ratio k_L/d_b as the essential component of a gas transfer coefficient (k_La) and multiplying by $Sc^{1/2}$, where $Sc = v/D$ is a Schmidt number, to bring k_La values to a reference temperature,[23] results in the final column in Table 2. The perforated plate sparger can be seen to provide the most effective gas transfer rate and the coarse bubble sparger the least effective gas transfer rate. Comparing the median of P1 through P4 with the median of P5 through P8 in Table 2 indicates that the airlift reactor is approximately four times more effective at gas transfer than the bubble column, under otherwise similar operating conditions.

The data of Table 2 were fit to a number of predictive equations, including the theoretical equation of Azbel[28] and an empirical equation for large drops in unstirred solution[33] to predict k_L. The data from the course bubble sparger and soaker hose were given twice the weight of the perforated plate data in the regression, because there were more of the perforated plate data and it was undesirable to have this sparger type dominate the regression. The Reynolds number dependence in the experimental data was over-predicted by both equations. The following relationship was most successful in representing the experimental data:

$$Sh = 7.6 Sc^{1/2} Re^{1/6} Bn^{-1/4} \tag{20}$$

where $Sh = k_L d_b/D$ is a Sherwood number, $Bn = \rho_l g d_b^2/\sigma$ is a Bond number, and $Re = u_g d_b/(v P_{gi}/P_{atm})$ is a Reynolds number. The term P_{gi}/P_{atm} is included in the Reynolds number to adjust the superficial gas velocity to sparger depth, where P_{gi} is the pressure at gas injection v is the liquid kinematic viscosity, σ is interfacial surface tension, and g is the acceleration of gravity. The exponent on the Schmidt number was assumed, because the parameters were not varied sufficiently to perform a curve fit, and the $Sc^{1/2}$ relation is generally used for bubbles with a diameter greater than 0.5 mm.[16] The fit of the data is shown in Figure 10, where both axes are divided by a Peclet number, $Pe = u_g d_b/D$, to spread the data, resulting in a Stanton number, $St = k_L/u_g$.

The Reynolds number is indicative of a turbulence effect upon the liquid film coefficient, and the Bond number is the ratio of buoyancy forces on the bubble and surface tension forces. In these experiments, the Bond number serves to reveal the liquid film coefficient dependence on bubble diameter because the variation in surface tension was relatively small. The exponent on the Reynolds number in Eq. 20 is lower than for many expressions representing experimental data from various arrangements.[20] Bubble dynamics in a deep airlift reactor and a deep bubble column seem to stabilize around a given bubble size and rise velocity in this bubbly flow regime.[18] An apparent result is that there is only a minor influence of the superficial gas velocity on liquid film coefficient. Although the bubble slip velocity should be important in determining k_L, its variation in these experiments was insufficient to elucidate dependence.

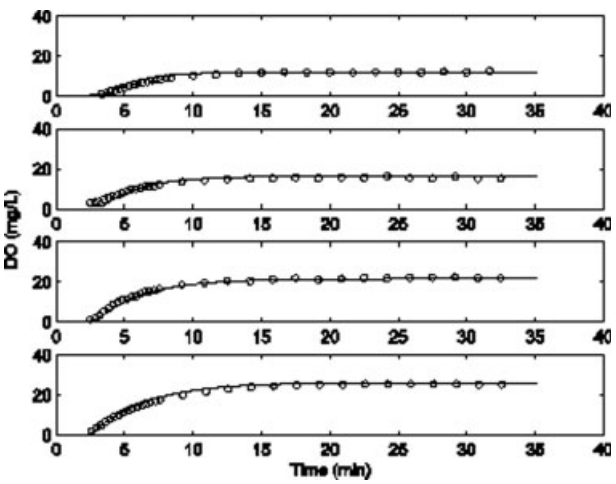

Figure 9. Comparison of the DO raw data (circles) with the best model fit (solid line) for the 10.6-m airlift reactor using a perforated plate at u_g = 0.01 m/s.

Measurement heights are at 22.0, 15.8, 9.5, and 3.0 m from top to bottom, respectively.

Table 2. Results for All Sets of Operating Conditions Given in Table 1

Exp.	U_r (m/s)	$d_b \times 10^3$ (m)	D_L (m^2/s)	P_{gi}/P_{atm}	$k_L \times 10^3$ (m/s)	Std. Err./C_f (%)	$k_L/d_B \times S_C^{1/2} \times 10^3$ (/s)
P1	0.25	2.44	0.039	3.26	0.21	2.07	0.43
P2	"	"	0.052	"	0.21	3.10	0.39
P3	"	"	0.059	"	0.41	3.14	0.70
P4	"	"	0.070	"	0.22	2.77	0.38
S1	0.24	2.28	0.040	"	0.15	1.27	0.33
S2	"	"	0.044	"	0.13	1.44	0.28
S3	"	"	0.052	"	0.16	2.37	0.33
S4	"	"	0.059	"	0.29	1.86	0.55
C1	0.23	2.76	0.050	"	0.08	1.24	0.13
C2	"	"	0.064	"	0.07	2.55	0.10
C3	"	"	0.072	"	0.10	2.21	0.14
C4	"	"	0.083	"	0.12	1.63	0.15
P5	0.22	3.84	0.097	"	0.08	2.63	0.07
P6	"	"	0.068	"	0.09	2.09	0.10
P7	"	"	0.080	"	0.11	2.27	0.11
P8	"	"	0.093	"	0.16	1.86	0.14
P9	0.19	2.32	0.033	2.03	0.24	1.20	0.56
P10	"	"	0.041	"	0.20	1.35	0.41
P11	"	"	0.045	"	0.19	1.40	0.38
P12	"	"	0.048	"	0.18	1.31	0.34
P13	"	"	0.052	"	0.19	1.15	0.35
P14	"	2.60	0.028	1.64	0.46	0.40	0.94
P15	"	"	0.033	"	0.34	0.52	0.65
P16	"	"	0.035	"	0.33	0.45	0.61
P17	"	"	0.037	"	0.29	0.43	0.51
P18	"	"	0.041	"	0.23	0.48	0.39

Values of bubble rise velocity (U_r) were fit to measurements of void ratio,[2] and values of d_B were measured as described in Giovannettone.[2] P_{gi}/P_{atm} is the pressure at gas injection relative to atmospheric pressure. Std. Err./C_f is the standard error of the curve fit for k_L normalized by the final concentration near the water surface. The final column gives the k_La normalized by the Sauter mean bubble diameter and referenced to a specific temperature.

Conclusions

Experiments were performed in a deep external airlift reactor and bubble column to determine how dispersion and gas transfer rates are affected in the bubbly flow regime by the measurement depth, gas flow rate, sparger type, and column type. A deep column of 23.4 m was chosen so that errors made due to scale-up to typical field/industrial column depths are minimized.

It was found that dispersion increases with superficial gas velocity for the gas velocities tested (0–0.01 m/s), which is in contrast to the results of Verlaan et al.,[34] who concluded that bubbles have little effect on liquid dispersion, but only considered superficial gas velocities above 0.014 m/s. Both the airlift reactor and the bubble column exhibited greater than a factor of 10 increase in dispersion with superficial gas velocities between 0.01 and 0.1 m/s. It was also concluded that an increase in the total unaerated depth of the water will cause an increase in the total dispersion throughout the height of the column, while the type of sparger used does not have a substantial impact. A slight difference was seen in the dispersion measured using the soaker hose, with a more uniform distribution of bubble size at higher gas flow rates.

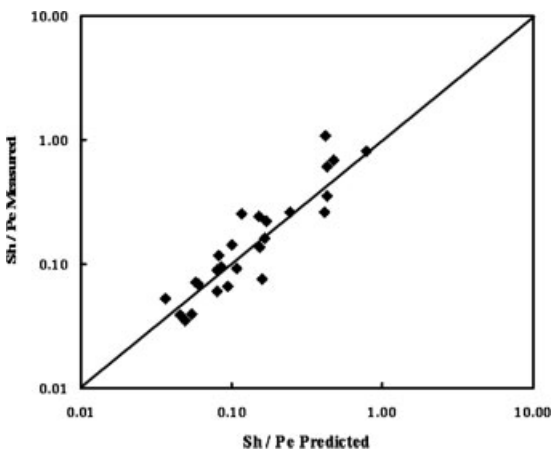

Figure 10. Measured values of *Sh/Pe* compared with those predicted by Eq. 20.

More contrast in mixing can be found when comparing column types. Maximum mixing occurred in the bubble column at a superficial gas velocity of 0.001 m/s, and then decreased to a minimum at 0.003 m/s, after which it increased at a rate similar to the airlift reactors. This maxima–minima pattern vs. superficial gas velocity did not occur in the airlift reactors. Overall, mixing in the bubble column was found to be greater than that in the airlift reactors at all superficial gas velocities tested. This further demonstrates that giving the column a small circulation velocity, which decreases the void ratio and bubble diameter, also causes decreased mixing. This will increase the efficiency of gas transfer in the reactor.

Gas transfer was quantified through measurements of DO concentration at several depths under different operating conditions in the airlift reactor and the bubble column. As was reported by Alvarez-Cuenca et al.,[3] much of the gas transfer was found to occur near the bottom of the reactor. DO profiles were fit to an explicit computational model to determine a liquid film coefficient, k_L. It was assumed that k_L is constant with measurement height, and therefore, one k_L value was used to represent the entire column for each set of oper-

ating conditions. The value of k_L increased as the total unaerated height of the airlift reactor decreased from 23.4 to 6.6 m. This indicates that measurements taken in smaller columns will tend to overestimate the amount of gas transfer if applied to field/industrial-scale columns. The perforated plate and soaker hose had the highest k_L, whereas the coarse bubble diffuser exhibited the lowest. This result suggests that k_L increases as pore size decreases and pore number increases, up to a given pore size, which is in agreement with the conclusions made using smaller columns.[4,6,12] It is interesting to note that the relative difference in k_L between spargers is greater than the difference in Sauter mean bubble diameter.

Substantial variation in the liquid film coefficient was found when comparing the bubble column to the airlift reactor. In a direct comparison of the bubble column and airlift reactor using the perforated plate, the median k_L of four experiments for each was 1.0×10^{-4} and 2.6×10^{-4} m/s, respectively. Combined with the larger Sauter mean diameter of the bubble column, this result indicates that the bubble column has a gas transfer coefficient, k_La, that is approximately one-fourth of the airlift reactor, even with the low superficial liquid velocity of 0.02 m/s.

The resulting k_L values for each set of operating conditions were characterized by Sherwood, Schmidt, Bond, and Reynolds numbers. The latter used the superficial gas velocity at the sparger depth. The exponent on the Reynolds number was lower than for other studies of liquid film coefficient in various experimental conditions. Because conditions in the deep airlift reactor and bubble column, under the operating conditions tested, stabilized around a given bubble size and rise velocity, there was only a minor effect of superficial gas velocity on the liquid film coefficient. The effect of bubble diameter on the liquid film coefficient was found to be $k_L \sim d_b^{-4/3}$.

The overall results of this study can be directly applied to field and industrial-sized columns operating in the bubbly-flow regime without the need for scale-up. To maximize mixing, a tall bubble column is recommended, while the type of sparger used is not important. If higher gas transfer efficiency is desired, an airlift reactor is recommended. Taller airlift reactors will have a lower k_La than shorter ones. Finally, a sparger containing many smaller holes, such as a perforated plate, should be used as opposed to one with fewer and larger holes, such as a coarse bubble diffuser.

Acknowledgments

The authors thank the Chicago District and the Engineering Research Center of the US Army Corps of Engineers for the necessary funding for this research, Grant W81EWF-4166-7569, and by the US Department of Education GAANN program in the form of a research fellowship. They also thank Ben Erickson and the shop crew at St. Anthony Falls Laboratory for the setup that made this study possible.

Notation

a = interfacial surface area of bubbles, m^{-1}
A = cross-sectional area, m^2
A_b = bubble surface area, m^2
Bn = Bond number ($\rho g d_b^2/\sigma_l$)
Bo = Bodenstein number ($u_l h_r/D_L$)
C = constituent concentration in the liquid, mg/L
C^* = constituent liquid concentration in equilibrium with the bubbles, mg/L
C_s = constituent saturation liquid concentration under standard atmospheric conditions, mg/L
Co = Courant number ($U\Delta t/\Delta z$)
d_b = Sauter mean bubble diameter, m
D = gas diffusivity, m^2/s
D_c = column diameter, m
Di = Dispersion number ($D_L\Delta t/\Delta z^2$)
D_L = longitudinal liquid dispersion coefficient, m^2/s
f = Darcy–Weisbach friction factor
g = gravitational acceleration, m/s^2
h = water height, m
H = Henry's Law constant, bars mol^{-1} L
k_L = liquid film coefficient, m/s
k_La = gas transfer coefficient, s^{-1}
P = pressure, atm
Pe = Peclet number ($u_g d_b/D$)
Q_g = gas flow rate, m^3/s
Re = Reynolds number ($u_g d_b/(\nu P_{gi}/L_{atm})$)
Sc = Schmidt number (ν/D)
Sh = Sherwood number ($k_L d_b/D$)
t = time, s
t_r = recirculation time, s
T = temperature, °C
u = superficial velocity, m/s
u^* = shear velocity near the walls, m/s
U = characteristic velocity, m/s
U_r = bubble rise velocity relative to u_l, m/s
V = column volume, m^3
V_b = total bubble volume, m^3
y = ratio of oxygen to nitrogen concentrations in the bubbles, $kmolO_2\ kmolN_2^{-1}$
z = vertical distance from the column bottom, m

Greek letters

γ = initial dye layer thickness, m
ν = liquid kinematic viscosity, m^2/s
ρ = density, kg/m^3
σ_l = interfacial gas/liquid surface tension, N/m
ϕ_g = gas void ratio (dimensionless)
Δt = time interval, s
Δz = chamber height, m

Subscripts

atm = local atmospheric
atms = standard atmospheric conditions
b = bubble
d = downcomer
f = final
g = gas
gi = location of gas injection
i = measurement index
in = initial condition
l = liquid
N = nitrogen
O = oxygen
r = riser
S = free surface
SN = nitrogen saturation
SO = oxygen saturation
ss = steady-state
vapor = water vapor

Abbreviations

BC = bubble column
DN = dissolved nitrogen
DO = dissolved oxygen
EALR = external airlift reactor
LDV = laser doppler velocimetry
TDG = total dissolved gases

Literature Cited

1. Singleton VL, Little JC. Designing hypolimnetic aeration and oxygenation systems—a review. *Environ Sci Technol*. 2006;40: 7512–7520.
2. Giovannettone JP. Hydrodynamics of a Two-Phase Flow in a Deep Airlift Reactor. PhD Thesis, University of Minnesota, Minneapolis, Minnesota, 2005.
3. Alvarez-Cuenca M, Baker CGJ, Bergougnou MA. Oxygen mass transfer in bubble columns. *Chem Eng Sci*. 1980;35:1121–1127.
4. Demoyer CD, Wilhelms SC, Gulliver JS. Comparison of submerged aerator effectiveness. *Lake Reserv Manage*. 2001;17:139–152.
5. McWhirter JR, Hutter JC. Improved oxygen mass transfer modeling for diffused/subsurface aeration systems. *AIChE J*. 1989;35:1527–1534.
6. Schierholz EL, Gulliver JS, Wilhelms SC, Henneman HE. Gas transfer from air diffusers. *Water Res*. 2006;40:1018–1026.
7. Demoyer CD, Schierholz EL, Wilhelms SC, Gulliver JS. Impact of bubble and free surface oxygen transfer on diffused aeration systems. *Water Res*. 2003;37:1890–1904.
8. Wilhelms SC, Martin SK. Gas transfer in diffused bubble plumes. In: Jenning SM, Bhowmik NG, editors. *Hydraulic Engineering: Saving a Threatened Resource-In Search of Solutions*. New York, NY: American Society of Civil Engineers, 1992:317–322.
9. Bello RA, Robinson CW, Moo-Young MB. Gas holdup and overall volumetric oxygen transfer coefficient in airlift contactors. *Biotechnol Bioeng*. 1985;27:369–381.
10. Bovonsombut S, Wilhelm A-M, Riba J-P. Influence of gas distributor design on the oxygen transfer characteristics of an airlift fermenter. *J Chem Technol Biotechnol*. 1987;40:167–176.
11. Choi KH, Lee WK. Circulation liquid velocity, gas holdup and volumetric oxygen transfer coefficient in external-loop airlift reactors. *J Chem Technol Biotechnol*. 1993;56:51–58.
12. Deckwer W-D, Burckhart R, Zoll G. Mixing and mass transfer in tall bubble columns. *Chem Eng Sci*. 1974;29:2177–2188.
13. Mavinic DS, Bewtra JK. Mass transfer of oxygen in diffused aeration systems. *Can J Civil Eng*. 1974;1:71–84.
14. Shimizu K, Takada S, Takahashi T, Kawase Y. Phenomenological simulation model for gas hold-ups and volumetric mass transfer coefficients in external-loop airlift reactors. *Chem Eng J*. 2001;84: 599–603.
15. Shimizu K, Takada S, Minekawa K, Kawase Y. Phenomenological model for bubble column reactors: prediction of gas hold-ups and volumetric mass transfer coefficients. *Chem Eng J*. 2000;78:21–28.
16. Wongsuchoto P, Charinpenitkul T, Pavasant P. Bubble size distribution and gas-liquid mass transfer in airlift contactors. *Chem Eng J*. 2003;92:81–90.
17. Ohkawa A, Kawai Y, Kusabiraki D, Sakai N, Endoh K. Bubble size, interfacial area and volumetric liquid-phase mass transfer coefficient in downflow bubble columns with gas entrainment by a liquid jet. *J Chem Eng Jpn*. 1987;20:99–101.
18. Deckwer W-D. *Bubble Column Reactors*. Cambridge, UK: Cambridge University Press, 1974.
19. American Society of Civil Engineers. *Standard for the Measurement of Oxygen Transfer in Clean Water*. New York, NY: ASCE, 1992.
20. Cussler E. *Diffusion: Mass Transfer in Fluid Systems*, *2nd ed*. Cambridge, MA: Cambridge University Press, 1997.
21. Ohki Y, Inoue H. Longitudinal mixing of the liquid phase in bubble columns. *Chem Eng Sci*. 1970;25:1–16.
22. Levenspiel O. *Chemical Reaction Engineering*. New York, NY: Wiley, 1972.
23. Gulliver JS, Thene JR, Rindels AJ. *Indexing gas transfer measurements in self-aerated flows*. *J Environ Eng*. 1990;116:503–523.
24. Kago T, Sasaki Y, Kondo T, Morooka S, Kato Y. Gas holdup and axial dispersion of gas and liquid in bubble columns of homogeneous bubble flow regime. *Chem Eng Commun*. 1989;75:23–38.
25. Fields PR, Slater NKH. Tracer dispersion in a laboratory air-lift reactor. *Chem Eng Sci*. 1983;38:647–653.
26. Gavrilescu M, Tudose RZ. Mixing studies in external-loop airlift reactors. *Chem Eng J*. 1997;66:97–104.
27. Taylor GI. The dispersion of matter in turbulent flow through a pipe. *Proc R Soc London Ser A*. 1954;223:446–468.
28. Azbel D. *Two-Phase Flows in Chemical Engineering*. Cambridge, MA: Cambridge University Press, 1981.
29. Isihara A. Determination of molecular shape by osmotic measurement. *J Chem Phys*. 1950;18:1446–1449.
30. Kataoka H, Takeuchi H, Nakao K, Yahi H, Tadaki T, Otake T, Miyauchi T, Washimi K, Watanabe K, Yoshida F. Mass transfer in a large bubble column. *J Chem Eng Jpn*. 1979;12:105–110.
31. Calderbank PH, Moo-Young MB. The continuous phase heat and mass-transfer properties of dispersion. *Chem Eng Sci*. 1961;16:39–54.
32. Akita K, Yoshida F. Bubble size, interfacial area, and liquid-phase mass transfer coefficient in bubble columns. *Ind Eng Chem Process Des Dev*. 1974;13:84–91.
33. McCabe WL, Smith JC. *Unit Operations of Chemical Engineering*, *3rd ed*. New York, NY: McGraw-Hill, 1976.
34. Verlaan P, Van Eijs AMM, Tramper J, Van't Riet K. Estimation of axial dispersion in individual sections of an airlift-loop reactor. *Chem Eng Sci*. 1989;44:1139–1146.

Manuscript received Oct. 22, 2007, and revision received Dec. 18, 2007.